



**HAL**  
open science

## Spreading and drying impact on printed pattern accuracy due to phase separation of a colloidal ink

Zhi Tao, Brice Le Borgne, Tayeb Mohammed-Brahim, Emmanuel Jacques,  
Maxime Harnois

► **To cite this version:**

Zhi Tao, Brice Le Borgne, Tayeb Mohammed-Brahim, Emmanuel Jacques, Maxime Harnois. Spreading and drying impact on printed pattern accuracy due to phase separation of a colloidal ink. *Colloid and Polymer Science*, 2018, 296 (11), pp.1749-1758. 10.1007/s00396-018-4372-1 . hal-01894675

**HAL Id: hal-01894675**

**<https://univ-rennes.hal.science/hal-01894675>**

Submitted on 15 Oct 2018

**HAL** is a multi-disciplinary open access archive for the deposit and dissemination of scientific research documents, whether they are published or not. The documents may come from teaching and research institutions in France or abroad, or from public or private research centers.

L'archive ouverte pluridisciplinaire **HAL**, est destinée au dépôt et à la diffusion de documents scientifiques de niveau recherche, publiés ou non, émanant des établissements d'enseignement et de recherche français ou étrangers, des laboratoires publics ou privés.

# Spreading and Drying Impact on Printed Pattern Accuracy Due to Phase Separation of a Colloidal Ink

Zhi Tao <sup>a,b</sup>, Brice Le Borgne <sup>a</sup>, Tayeb Mohammed-Brahim <sup>a</sup>, Emmanuel Jacques <sup>a</sup>,

Maxime Harnois <sup>a,\*</sup>

<sup>a</sup> Institut d'électronique et des Télécommunication de Rennes, UMR CNRS 6164, Université de Rennes 1, Campus de Beaulieu, 35042 RENNES Cedex (France)

<sup>b</sup> School of Electronic Science and Engineering, Southeast University, Nanjing 210096, People's Republic of China

---

## Abstract

Drop-on-demand inkjet printing relies on the dispensing and precise positioning of very small amount of liquid on substrate before its transformation to a solid. Consequently, many steps are involved during inkjet printing process that must be understood to fabricate accurate patterns. In this work, multicomponent colloidal mixture spreading and drying is investigated. A systematic study has been performed to explain the impact of the jetting frequency, the drop spacing and the substrate exposure to UV ozone on a colloidal silver ink behavior. It is demonstrated that phase separation between stabilizing agent and colloids can occur during the spreading step. This phenomenon is described and appears to be related to the colloidal nature of the ink. It is shown that it can have a negative impact on patterns accuracy and several routes are given to overcome these issues.

Keywords: Inkjet Printing; Printed Patterns Accuracy; Colloidal Ink; Phase Separation; Ink Drying

---

## 1. Introduction

Additive Manufacturing (AM) has gained a growing interest throughout the past decades in new application fields such as optoelectronics,<sup>[1-4]</sup> ceramics,<sup>[5, 6]</sup> biotechnology,<sup>[6, 7]</sup> organic light emitting devices,<sup>[6, 8]</sup> field effect transistors,<sup>[6, 9, 10, 11]</sup> solar cells,<sup>[6, 12]</sup> flexible and stretchable interconnects.<sup>[13, 14]</sup> It is now well-established that AM technology such as inkjet printing, provides a breakthrough compared to the existent subtractive technologies.<sup>[6, 15, 16]</sup> One of the inkjet printing techniques, called drop-on-demand (DoD) printing, relies on the coalescence of adjacent droplets that are expelled from nozzles onto a substrate.<sup>[17, 18, 19]</sup> Picoliters droplets volume are now easily

printed using commercial printers and many functional inks are on the shelves.<sup>[9, 20]</sup> Indeed, many materials such as nano-objects,<sup>[9, 21, 22, 23]</sup> polymers,<sup>[24, 25, 26]</sup> organic/inorganic semiconductors<sup>[27, 28]</sup> have been solubilized in order to design conductive, insulating or semi-conductive inks, respectively, leading to active or passive devices fabrication.<sup>[29]</sup>

Inkjet printing process is composed of three main steps: i) droplet generation, ii) droplet spreading onto an arbitrary substrate and iii) droplet drying. Each step have to be fully understood in order to fabricate accurate patterns.<sup>[9]</sup> Consequently, literature is replete of work dealing with each step optimization. Concerning droplet generation, recent works have demonstrated the exploitation of a jettable window (i.e., using Ca-We space) to adjust the rheology of nanoparticle ink<sup>[20]</sup> or polymeric ink<sup>[13]</sup> to allow the design of a jettable ink. Using such methodology, nozzle clogging, long-lived filament, and satellite droplets can be suppressed improving pattern accuracy.<sup>[30, 31, 32]</sup> However, the patterns generation behavior remains complex to understand because many experimental parameters play a crucial role during ink spreading and drying, due to its interaction with the substrate. For instance, lines can show uniform, bulged, scalloped, stacked or separated patterns as function of jetting frequency and drop spacing.<sup>[33, 34]</sup>

After the drying step, droplets often show non-uniform profile that is frequently attributed to the so-called coffee stain effect, firstly described by Deegan.<sup>[35]</sup> Moreover, several works proposed strategies to suppress such undesirable behavior.<sup>[9, 36, 37]</sup> Consequently, patterns profile can be optimized from smooth to periodically wave-shaped film depending on application requirements.<sup>[9, 36, 38]</sup>

On the one hand, new inks designs are more and more complex and multicomponent mixtures are usually required to obtain jettable inks fitting desired properties (e.g., high conductivity for colloidal ink).<sup>[39]</sup> On the other hand, literature dealing with multicomponent mixture reports more complex droplets drying behavior than in the work of Deegan.<sup>[40, 41, 42]</sup> Indeed, these works that mainly dealt with isolated drop-casted microliters droplets, have shown the presence of phase separation during spreading and drying. In our work, this behavior has been verified on picoliters printed droplets as function of substrate wettability. Moreover in the second part of this work, ink phase separation impact on patterns formation such as lines or squares is studied. Indeed, in the field of printed electronics, lines or squares are required to fabricate interconnects or electrodes for instance.

## 2. Results and discussion

A commercial colloidal based silver ink (ANP 40LT15C) has been used as received. Note that, this ink is frequently used for numerous printed electronics applications. Its chemical composition has been kept constant for all the study. The wetting behavior of substrates has been controlled using UV-ozone treatment. Droplets of silver based ink have been printed on 400 nm thick polymeric film (epoxy photoresist: Su8 2002 Microchem) using spin coating technique. Su8 films offer high chemical resistance and structural stability.<sup>[43]</sup> Moreover, it allows the fabrication of electronic devices.<sup>[44]</sup>

Jetting parameters have been optimized to respect the jetting criteria (e.g., no satellite droplets...) described in experimental section. The inkjet printing parameters such as: velocity, firing voltage, substrate temperature have been kept constant and equal  $3\text{m}\cdot\text{s}^{-1}$ , 65V and  $50^\circ\text{C}$ , respectively. Jetting behavior of silver ink is shown in supplementary **video S1**. This crucial step is prerequisite in order to study the accuracy of the printed pattern.

### a. Droplet spreading

The effect of the substrate surface wetting properties on the droplets drying behavior has been studied as function of its UV ozone exposure time (see in **figure 1**). The substrate has been exposed to UV ozone time ranging from 0 to 10 minutes and printing has been performed immediately after UV ozone treatment. As shown in **figure S1**, surface treatment has increased Su8 surface hydrophilicity. Indeed, water contact angle values have varied over a wide range, from hydrophobic (water contact angle equals at least  $90^\circ$ ) to hydrophilic behavior (water contact angle value is less than  $40^\circ$ ). Consequently, Su8 film has been chosen to deeply highlight the impact of UV ozone exposure effect. **Figure 1a** shows three optical pictures, highlighting the effect of UV ozone onto droplets drying behavior. Aggregated silver nanoparticles are highlighted by a light yellow region delimited by the mark: "Inner ring". As expected, UV ozone exposure time has a strong impact on the silver nanoparticles spreading. The more the surface has been exposed to UV ozone, the more the droplet has spread and consequently the more the region covered with nanoparticles is large. Surprisingly, two different droplet drying behaviors can be distinguished as function of UV ozone exposure time. At low UV exposure time (1 minute), only the inner ring can be observed. At higher UV ozone exposure times (6 and 10 minutes) another ring, marked "outer ring", was observed. Such phenomena will be discussed in the next section. Moreover, UV ozone exposure time has also an impact on the two dimensional profile of dried droplet. **Figure 1b** shows

these dried droplets morphologies as function of UV ozone exposure time in order to highlight the evolution of their two dimensional profiles. **Figure 1c** shows corresponding diameters values extracted from figure 1b.

After 4 minutes UV ozone exposure time, both diameters (inner and outer ring) have no significant evolution. Outer ring cannot be observed before 4 minutes UV exposure time whereas inner ring diameter increases. Moreover, UV ozone exposure time have a strong impact on colloids layer thickness and morphology. Indeed, 10 minutes UV ozone exposure time divides the average thickness by more than 2 and exacerbates the well-known coffee stain effect.<sup>[35]</sup> Moreover, outer diameter is thicker and larger for 10 minutes of UV exposure time than for 6 minutes.

In conclusion, at low UV ozone exposure time (less than 4 minutes) the behavior of colloidal drying can be described, in first approximation, using Deegan's work.<sup>[35]</sup> This phenomenon, known as "coffee stain", is due to the solvent evaporation rate which is greater at the surroundings of the so-called "triple contact line". Consequently, when the contact line is pinned, solute transport from the center to the edge is induced by replenish flow, leading to inhomogeneous films after complete evaporation. However, as previously described, droplets drying behavior is different when the surface becomes highly hydrophilic (i.e., at higher UV ozone exposure time). In this case, Deegan's theory cannot fully explained the drying behavior.

A relevant study has reported the creation of a hydrophobic layer that surrounds (i.e., outer ring) printed patterns (e.g., isolated droplets) on a hydrophilic substrate.<sup>[45]</sup> This study showed that upon the impact, the droplet spreads at it maximum value before receding to its equilibrium state. Consequently, during triple contact line receding step, the desorbed stabilizing agent (hexadecylamine, in their case) was deposited leading to a hydrophobic boundary around the printed patterns. Note that, in this study, no observations was performed to confirm this hypothesis. However, this interesting work has shown that the surrounding layer impacts patterns creation.

In our study, another hypothesis will be drawn to explain such phenomenon. It is based on other works that have studied the drying behavior of a complex mixture.<sup>[37, 40]</sup> Indeed, it has been proved that multicomponent mixtures are submitted to more complex internal flow than these ones studied in the work of Deegan, for instance (i.e., diluted colloids in a solvent). In our work, three components composed the silver based ink (see in experimental section: "materials"): i) hard silver nanoparticles, ii) solvent and iii) Polyvinylpyrrolidone, (PVP). Indeed, it has ever been demonstrated that the commercial ink (DGP 40LT15C) used in this study, reveals the presence of

carbonyl groups (FT-IR experiments), suggesting that a polymer ligand such as PVP, has been used.<sup>[46,47]</sup> Moreover, it is well-known that PVP is commonly used in nanoparticles based ink as surface stabilizer, growth modifier, nanoparticle dispersant, and reducing agent. The PVP avoids large sized nanoparticles agglomerations which can occur due to Van Der Waals or Coulomb's forces.<sup>[37, 40, 41]</sup> Indeed, nanoparticles agglomeration is a major drawback for inkjet printing because it drastically increases nozzles clogging and must be avoided.<sup>[21]</sup> Furthermore, as for the work dealing with hexadecylamine as stabilizing agent, we suggest that an amount of PVP adhered to silver thanks to carbonyl silver bound and another amount is free (desorbed).

Taking into consideration ink composition and the previously mentioned works dealing with multicomponent mixtures drying, an hypothesis can be drawn: during spreading and drying steps, the droplets show a formation of an inner "cap" and an outer "foot" (see in figure 3a), as described in other works.<sup>[40, 42]</sup> A phase separation can occur leading to a colloid rich and a polymer rich region located in the center and at the periphery of the droplet, respectively. We suggest that the polymer rich region is mainly composed of desorbed (free) PVP. In that case, colloidal particles that are confined in the central region, also called "gelation region", form a "solid-like particle gel" which resists to droplet internal flow.<sup>[40]</sup> Indeed, as the solvent evaporates, concentration of nanoparticles increases and consequently they approach each other until they aggregates due to strong van der Waals interactions.<sup>[40]</sup> Due to phase separation, polymer which are confined in the foot pinned the droplet and is accumulated at the contact line due to internal flow in the foot. Such a behavior leads to the final residue as shown in **figure 2**. Furthermore, **figure S2** (see in supplementary information) give more information about drying behavior inside the cap.

Equipment used to perform inkjet printing experiments does not allow to acquire top view images immediately when droplets land on substrate surface to verify this hypothesis. Moreover, due to the small droplet volume (fast evaporation) it is not possible to take the substrate out of the equipment in order to fully analyze spreading and drying behavior. Consequently, spreading and drying analyze have been performed on 0.1  $\mu\text{L}$  droplet deposited using micropipettes under microscope to mimic the phenomena. Top view optical pictures acquired as function of time are shown in figure 3. Images in figures 3a to 3e show the spreading behavior of the droplet onto Su8 surfaces exposed to 6 minutes of UV-ozone. During droplets spreading, materials are not uniformly distributed and two advancing fronts can be observed: the first one is relative to the triple contact line and the second one corresponds to the perimeter of the dark area. It confirms

that two phases exist in the droplet. Importantly, this observation highlights that the foot area is formed immediately after the droplet deposition and continually expands until the contact line is pinned (i.e, during the spreading step). Note that the dark area corresponds to a region rich in colloids. Colloids show replenish movement and never go outside this region that can suggest the existence of a gelation region. Upon drying, an iridescent region occurs in the foot area. Such observed behavior can highlight a gradient of material thickness. Taking into consideration previous observations, such region could be relative to polymer rich thin films. When spreading reaches its maximum, the triple contact line (first front) is pinned before it recedes letting the residue (figures 3f and 3e). Colloids rich region that has also been pinned (see figures 3g and 3h), dries at last step occurring a classical coffee stain. Consequently, the resulting dried profile (i.e., two rings) is obtained because of a stick-slip motion of the contact line. Indeed, contact line is mainly pinned two times during its receding phase and consequently lets residues of materials where it has been pinned. Note that the observation of the wetting and the drying behavior highlights that the residue is due to a combination of several physical phenomena, which is mainly due to phase separation occurring during droplet spreading and not only the stick-slip motion of the contact line. Note that, additional experiments could be performed to deeply analyze the outer ring regions using in situ X-rays as already shown by Riekel et al. [48, 49, 50]

The results presented in this section have shown that due to the presence of PVP molecules a residue remains at the periphery of the droplet triple contact line whereas colloids are confined in the central region. We have demonstrated that the control of the surface wetting properties is an easy way to drastically reduce such unexpected behavior. Note that, other ink composition using another stabilizer agent have also shown the existence of a surrounding layer. Moreover, it has also been shown that such a layer can have a strong impact on the pattern formation. That's why, in the following, deeper investigations will be performed on more complicated patterns (conductive lines and square shaped patterns) to understand the effect of such residue as function of the substrates wetting and the jetting frequency.

## **b. Patterns formation**

### **i. Lines behaviors**

DoD printing technique relies on the coalescence of adjacent droplets in order to form patterns. However, the substrate wettability control is a key parameter to obtain well-defined patterns.

Indeed, when triple contact line is not firmly pinned patterns can split during drying due to fluid instability as shown in supplementary **figure S3**. Thus, it is well-known that surface treatment (e.g., UV ozone) is necessary to solve this drawback. As previously highlighted, such a treatment will promote polymeric residue that could have an impact on pattern accuracy. Note that, numerous works report on printed lines drying behaviors. However, at our knowledge, no works have focused on the printed lines formations when a residue is accumulated at the triple line (outer ring). **Figure 4** shows the printed lines formation as function of surface wetting behavior and drop spacing (distance between the centers of two adjacent droplets).

Figures (4a, 4b, 4c, and 4d) show line formation behavior at low UV ozone exposure time (2 minutes). As expected, when the gap between droplets centers (drop spacing) is: higher than the droplets diameters, close to droplets diameters, well-adjusted or too close, it leads to isolated droplets, scalloped lines, well-defined lines or bulged lines, respectively. The origin of this phenomenon has ever been reported in literature and will not be detailed here. For UV exposure time equals 10 minutes (figures 4e, 4f, 4g, 4h), the same phenomenon occurs for isolated droplets (figure 4e) and scalloped lines (figure 4f). Well-defined lines can also be printed (figure 4g). However, even if drop spacing is drastically reduced (figure 4h), line does not show bulges. It seems that due to surface hydrophilicity (i.e., low water contact angle), inks spreads and consequently even if drop spacing is reduced, not enough materials is added to obtain bulges instabilities.<sup>[33, 34]</sup> Moreover, zoom in red hatched inset shows that outer ring is formed around the line independently of drop spacing value. This phenomenon can be explained as follows: a line is formed when at least two droplets coalesce. Indeed, a droplet falls down and begins to dry. Another one lands and merges with the first one. At high UV exposure time, the separation phase occurs when droplets dry. Consequently, PVP residue that remains at the triple contact when the first droplet is printed can be dissolved when the second one is printed. The same mechanism occurs until the last droplet of the line is printed. The case shown in figure 4f, well describes the phenomena. Indeed, when inter-droplet distance is higher than inner ring diameter but lower than outer ring diameter only the morphology of the outer ring is impacted during drying. In order to mimic this phenomena, two droplets have been successively drop casted using micropipette. Top view optical images acquired during droplet spreading and drying confirms the previously mentioned explanations (see in **figure S4**).

In conclusion, the same drying mechanism observed in the first section at droplet scale, also occurs when line dries. However, it does not drastically impact lines formation but PVP residue remains at periphery of the inner lines. In the next section, deeper investigations will be performed on square shaped patterns to highlight the impact of PVP residue on more complex patterns formation.

## **ii. Square shaped behaviors**

### **1. Systematic study**

Optical pictures in **figure 5** shows the impact of drop spacing, jetting frequency and UV ozone exposure time on printing accuracy of the printed square patterns. The squares are fabricated as follows: droplets are successively printed along x axis (from left to right) and coalesce to form a line. This printing scenario is repeated when the printhead has shifted along y axis, toward the top of the pictures. Consequently, lines coalesce and form the squares (for more details, see the 3D scheme in supplementary **figure S5**). Importantly, in this set of experiments each square are printed from the bottom left to the top right. The accuracy criterion is that patterns shape have to be a square (1mm×1mm) fully filled with silver.

This systematic study shows experimental parameters impact on printing accuracy. The jetting frequency, the drop spacing, the UV ozone exposure time have been varied. As shown in figure 5, whatever UV ozone exposure time is, three behaviors can be clearly distinguished: i) isolated droplets, ii) partially collapsed droplets and iii) merged droplets. Note that the drop spacing values have been carefully adjusted to highlight such well-known behaviors.

When UV ozone exposure time increases the patterns accuracy decreases independently of the jetting frequency or the drop spacing. Nevertheless, whatever UV ozone exposure time was, the patterns could be fully filled with ink (i.e., no fluidic instability). However, patterns are not well-defined even in the wide tested range of drop spacing and jetting frequency. This unexpected behavior needs to be clarified. In order to explain this behavior, deeper investigations on these two parameters influences have been performed.

### **2. Drop spacing study**

The first row (**figures 6a, 6b and 6c**) shows independent droplets (i.e., drop spacing is higher than droplet diameter). The second row (**figures 6d, 6e and 6c**) shows partially merged droplets (i.e., drop spacing value is close to the droplet diameter). The third row (**figures 6g, 6h and 6i**) shows

merged droplets (i.e., drop spacing value is lower than droplet diameter). Each column corresponds to a different UV ozone exposure time (2, 6 or 10 minutes from left to right).

As previously mentioned, film formation at low UV exposure time (first column) shows different behavior compared to the others columns due to PVP residue (“outer ring”) remaining when surface is highly hydrophilic. However, the first line residue impacts the second printed line. Such a phenomena is in good agreement with the supplementary figure S4 where the phenomena has been observed in real time under microscope. It is exacerbated when the drop spacing value decreases for the following reasons.

At high drop spacing (first row), in each cases, the three first printed lines show different spreading and drying behavior. In figure 6a, isolated droplets are observed because outer ring does not occur. Indeed, as already observed in figures 1b and c and discussed in previous sections, when UV ozone exposure time is lower than 4 minutes, the outer ring does not occur.

In figure 6b and 6c, PVP residue is observed but outer ring of each droplets that form a lines has collapsed but has no impact on inner ring of each droplets. In this case, PVP residue does not influence droplets shapes. However squares are not totally filled with ink.

In the second row, when the drop spacing is equal or slightly inferior to the droplets diameters (inner diameter), the outer ring of the previously printed droplets has not enough time to dry and to pin before its neighbour droplet has landed (figure 6e). This behavior occurs for all the droplet that form a line. However, when printing the second lines, the PVP residue of the first line is firmly pinned and consequently, induces deformation of the second line due to its 2 dimensional profile (see figures 6e and 6f). In this case, PVP residue does not influence the first printed lines but the others ones are impacted. Consequently, the square is not well-defined. Note that, the printing parameters that have been fixed in figure 6e are optimum to highlight such hypothesis. In the first line, droplets show circular shape partially collapsed, whereas, in the second line, droplets also collapsed but show semicircular shape. Note that the flat droplets vertex of the second line faces the first printed line, clearly showing the negative impact of PVP residue.

When drop spacing is inferior to droplet diameters (third row), the aforementioned phenomena occurs. Indeed, as inner ring of each droplets overlap square is more filled. However, as shown in figures 6h and 6i, PVP residue remains leading to square deformation. Such assertion is in good

agreement with the optical picture of figure 6g. Indeed, when no PVP residue occurs patterns are well-defined.

As highlighted in this section, the PVP residue influence on patterns formation occurs when such residue have enough time to be pinned. Consequently, could the increase of printing velocity (i.e. the increase of jetting frequency) pave the way to overcome this drawback?

### 3. Jetting frequency study

Experiments have been performed to highlight the impact of jetting frequency on square patterns formation. **Figure 7a** and **7b** show optical pictures of squares using the following experimental parameters. For both figures, drop spacing and UV exposure time are fixed and equals  $180\mu\text{m}$  and 10 minutes, respectively. Jetting frequencies varied and equal 20Hz and 3340Hz as shown in figure 7a and 7b, respectively.

At low jetting frequency (figure 7a), outer ring is formed around each line as usual. Interestingly, when printing frequency increases, as shown in figure 7b, outer ring is observed around the square but cannot be observed around each printed lines. In this case, outer ring formed around each lines has not enough time to be pinned. Consequently, the shape of each droplets inner ring are not impacted. Finally, PVP residue remains at the periphery of the square. Obviously, in this drop spacing conditions, square is not fully filled with ink. When the drop spacing is reduced (see figure 7c), the same phenomena occurs. Patterns accuracy are better when printing at high velocity (figure 7d) compare with those printed at lower frequency (figure 6i for instance). However, in these conditions holes remain. Such a phenomena could be due to a largest amount of PVP induced when printing at lower drop spacing. A way to solve this problem could be to increase printing velocity, however it was not possible with the printer used in this study.

### 3. Conclusion

On the basis of previously reported works dealing with multicomponent mixture, microliters scale drop can show phase separation when a multicomponent mixture is used.<sup>[40, 42]</sup> This work highlights that this phenomena can occur when PVP is used as stabilizer in colloidal based ink. It has been demonstrated that printed picoliters droplets and dropcasted microliters drops show the same morphology after drying. Indeed, an inner colloidal rich region and an outer polymer rich

region can be distinguished independently of deposition techniques. Moreover, the optical observation of the spreading and drying behavior confirm that a phase separation occurs. The new results observed in this work gave an alternative explanation of the phenomena already observed for another ink containing another kind of stabilizing agent.<sup>[45]</sup>

This complementary work gives more information for ink designer and experimenter involved in the field of printed electronics. Indeed, in the second part of this work, it has been demonstrated that PVP residue has a negative impact onto printed pattern accuracy, especially when the substrate became highly hydrophilic. Moreover, this work has highlighted one of the experimental condition (i.e., substrates wetting behavior) that exacerbates the phase separation of a complex mixture made of colloids and polymer ligand. This study could pave the way to other dealing with a systematical study of other experimental conditions such as: ligand kind of material, surface materials and or roughness. It should help to fully understand the phase separation that occurs during inkjet printing of colloids droplets.

#### **4. Materials and methods**

##### **a. Materials**

400nm thick Su8 2002 films were obtained using spin-coating (Velocity = 3000 rpm; Acceleration = 3000rpm.s<sup>-1</sup>, time = 60 seconds) on glass substrates. Su8 films were baked at 95°C and exposed to UV before the final baking at 110 during at 20 minutes. Jetlight equipment (UVO-Cleaner® 42) was used for UV ozone exposure. For SEM experiments, Su8 was spin coating following the same process. Silicon substrates was used and 5nm gold was deposited after inkjet printing step (silver based ink). Such protocol was used in order to reduce charging effect during SEM observations. All the experiments have been performed with the same Silver based ink that has been purchased from ANP and used as received. Ink reference is: ANP 40LT15C which is composed of Silver nanopowder, <100 nm particle size and contains PVP as dispersant (Sigma Aldrich). TGME (C<sub>8</sub>H<sub>18</sub>O<sub>4</sub>) is used as main solvent. The metal content, the surface tension, the viscosity and the density equal 30.18wt%, 36.8mN/m, 14.16cps, 1.45g/mL respectively.

##### **b. Jetting experiments:**

- **Jetting criteria**

The jettability criterion is the ability to obtain a droplet at a distance range ( $\Delta r$ ) between 800  $\mu\text{m}$  and 1 mm (acceptable working distance for the printer equipment: CERADROP Xseries). Satellite droplets or tail must be reabsorbed by the nozzle and jettability must be stable for a long time with low droplet misalignment on the substrate ( $\Delta x < 5 \mu\text{m}$ ). The stroboscopic vision system was used to determine droplet volume and velocity of three ink dilutions.

- **Jetting at low frequency**

For all the experiments, results obtained using 20Hz as jetting frequency show deformed printed patterns. In this case, jetting frequency is closed to the lowest printing velocity of the printer. Consequently, authors suggest that patterns deformations are only due to the printer.

**c. Characterization**

Scanning electron microscope images were obtained using a JEOL 7100 FEG microscope. Water contact angle measurements were obtained using Kruss DSA30 equipment. Data are an average value of 10 measurements. Profilometry measurements were performed using TENCOR KLA P6 equipment. Optical microscope images were obtained using a Leica microscope equipped with a digital camera. Optical images in figure 5 were obtained using digital camera of CERADROP Xseries equipment.

**FIGURES**

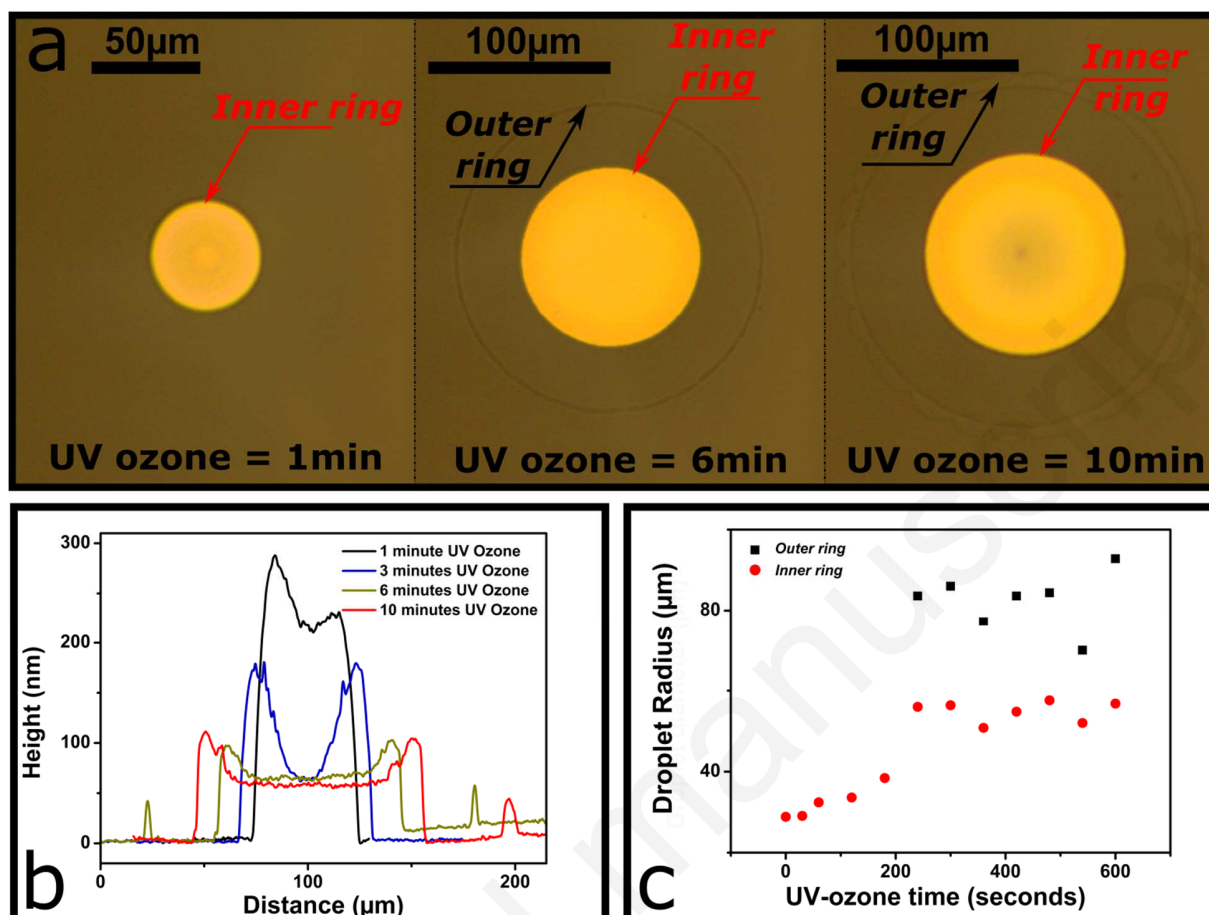


**Figure 1:** Morphological evolution of dried droplet as function of UV ozone effect. a) top view optical pictures of dried droplet as function of UV ozone time. UV ozone exposure time equals 1, 6 and 10 minutes (from left to right); b) Two dimensional profiles extracted along the diameter of a dried droplet as function of UV Ozone exposure time. UV ozone exposure time equals: 1, 3, 6 and 10 minutes; c) inner droplet diameter and outer droplet diameter as function of UV ozone exposure time.

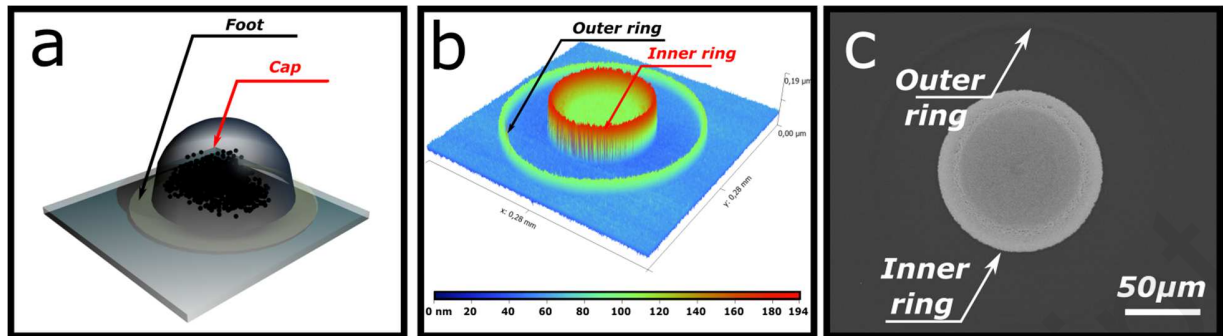


**Figure 2:** Drying behavior of droplet. a) 3D schematic of droplet at the beginning of drying step. A foot and a cap area occurs. b) 3D profiles showing outer and inner ring of a dried droplet on polymeric surface exposed to UV ozone (10 minutes). c) SEM picture showing dried droplet.

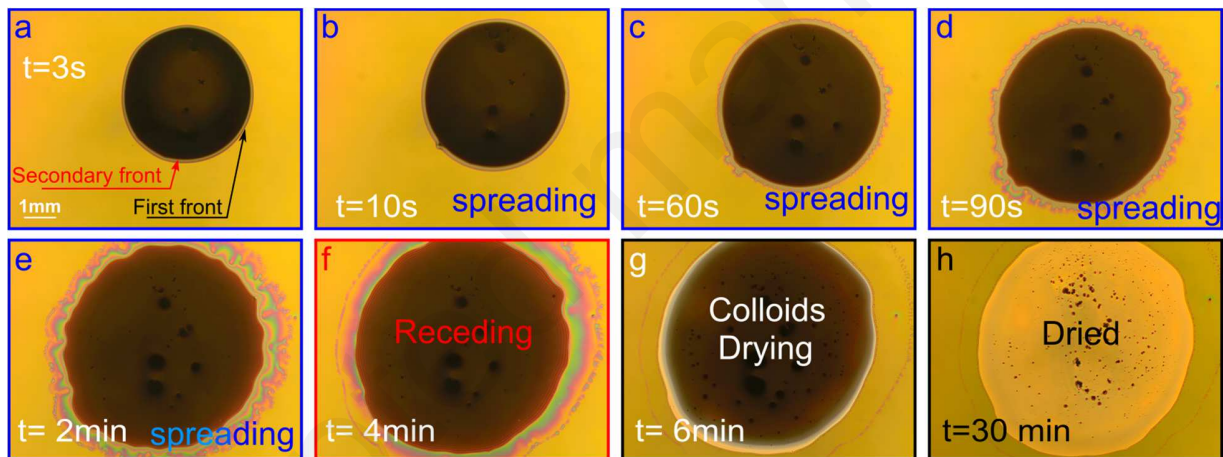


**Figure 3:** Optical images of silver ink drop-casted on Su8 surface exposed to 6 minutes UV-ozone. Images a) to d) show the drying behavior of the droplet as function of time. Images a) to h) have been captured respectively 3s, 10s, 60s, 90s, 2min, 4min, 6min and 30min, after the droplet deposition. From a) to d), two advancing fronts could be observed showing the separation phase when the droplet spreads. In figure f) the droplet contact line has been pinned and is beginning to recede. In figure g) the solvent has evaporated in the foot area and colloids area remains to dry. In figure h) the droplet is fully dry.

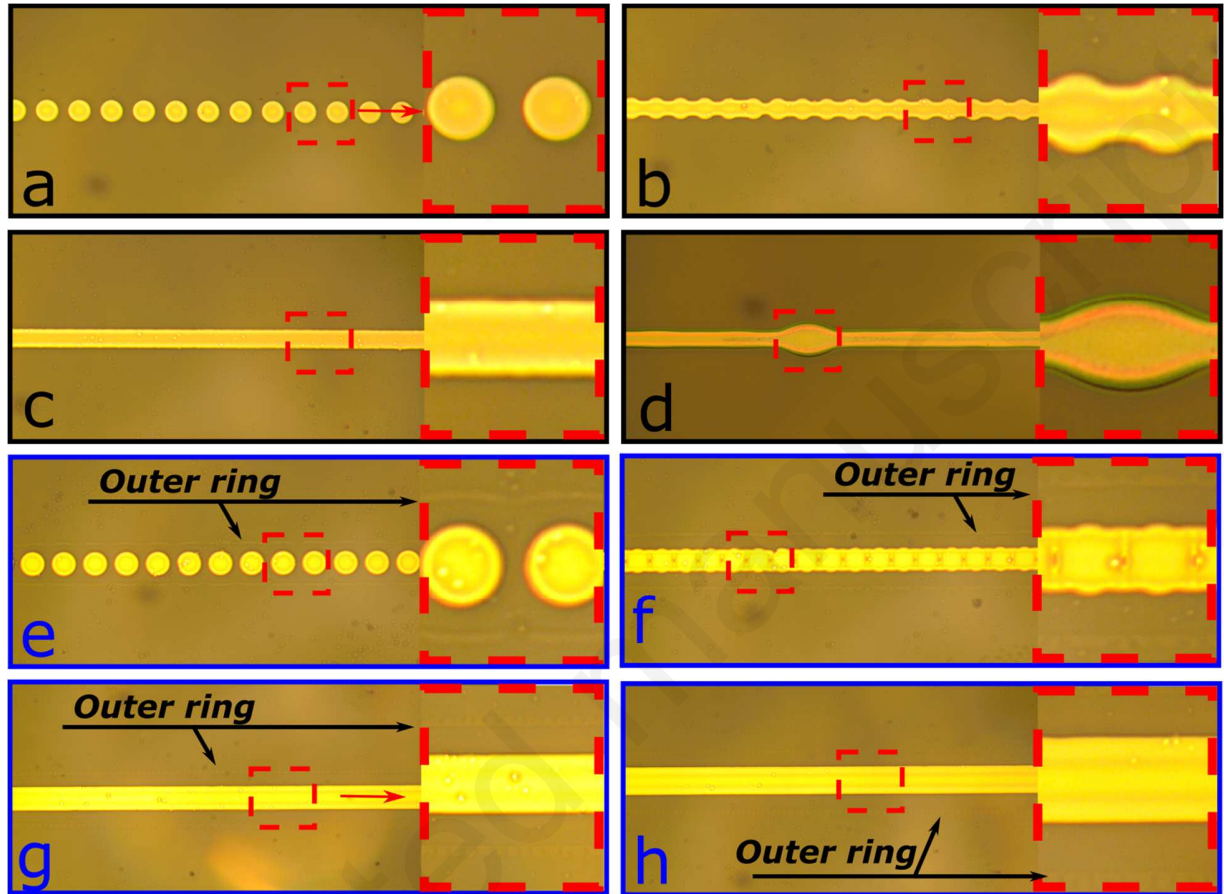


**Figure 4:** Lines formation mechanism as function of drop spacing and UV ozone exposure time. Jetting frequency equals 1 kHz. Hatched marks show zoom on lines. UV ozone time equals 2 minutes and drop spacing equals: a) 80 $\mu\text{m}$  leading to isolated droplets, b) 60 $\mu\text{m}$  leading to scalloped line, c) 40 $\mu\text{m}$  leading to well defined lines, d) 25 $\mu\text{m}$  leading to bulged line. UV ozone times equals 10 minutes and drop spacing equals: e) 200 $\mu\text{m}$  leading to isolated droplets, f) 130 $\mu\text{m}$  leading to scalloped lines, g) 70 $\mu\text{m}$  leading to well defined line, h) 60 $\mu\text{m}$  leading to well defined line.

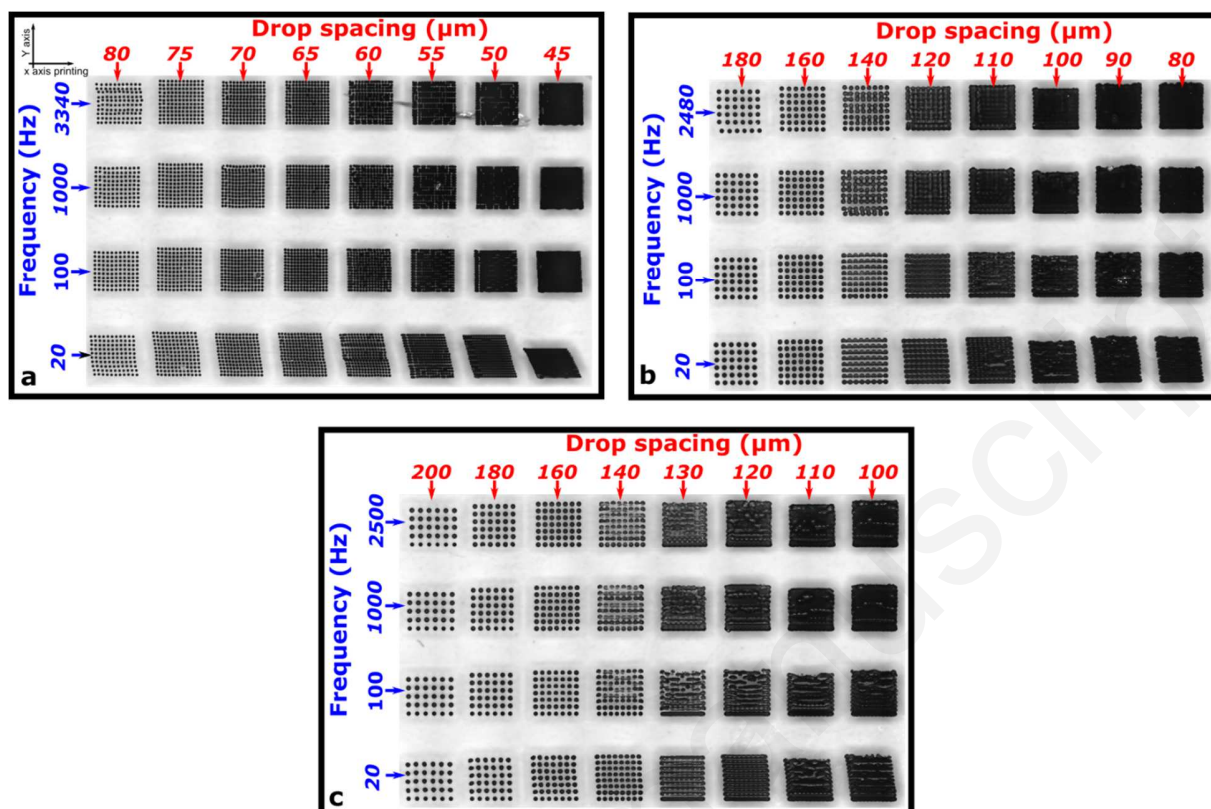


**Figure 5:** Square shaped patterns (approximately 1\*1mm) varying drop spacing, jetting frequency and UV ozone exposure time; a) UV ozone exposure time equal 2 minutes; drop spacing varies from 80 to 45 $\mu\text{m}$  and jetting frequency varies from 3340 to 20Hz; b) UV ozone exposure time equals 6 minutes; drop spacing varies from 180 to 80 $\mu\text{m}$  and jetting frequency varies from 2480 to 20Hz; c) UV ozone exposure time equal 10 minutes; drop spacing varies from 200 to 100 $\mu\text{m}$  and jetting frequency varies from 2500 to 20Hz.

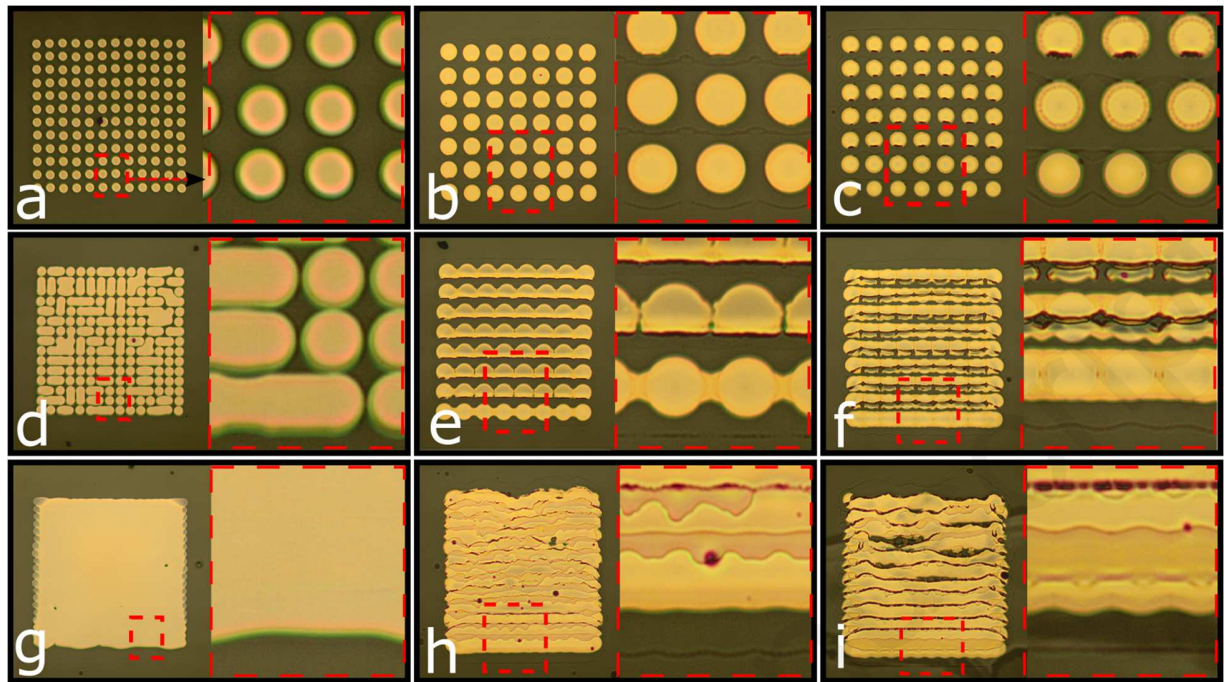


**Figure 6:** Optical pictures of square shaped patterns (approximately  $1 \times 1 \text{mm}$ ) printed at fixed jetting frequency equals  $100 \text{Hz}$  and varying:

- i) UV ozone exposure time equals: 2, 6 and 10 minutes shown in column 1, 2 and 3, respectively;
- ii) drop spacing in order to print: isolated droplets matrix, partially merged droplets, continues patterns shown in row 1, 2 and 3, respectively. Drop spacing experimental values equals: a)  $75 \mu\text{m}$ ; b)  $160 \mu\text{m}$ ; c)  $160 \mu\text{m}$ ; d)  $60 \mu\text{m}$ ; e)  $140 \mu\text{m}$ ; f)  $130 \mu\text{m}$ ; g)  $45 \mu\text{m}$ ; h)  $80 \mu\text{m}$ ; i)  $100 \mu\text{m}$ .

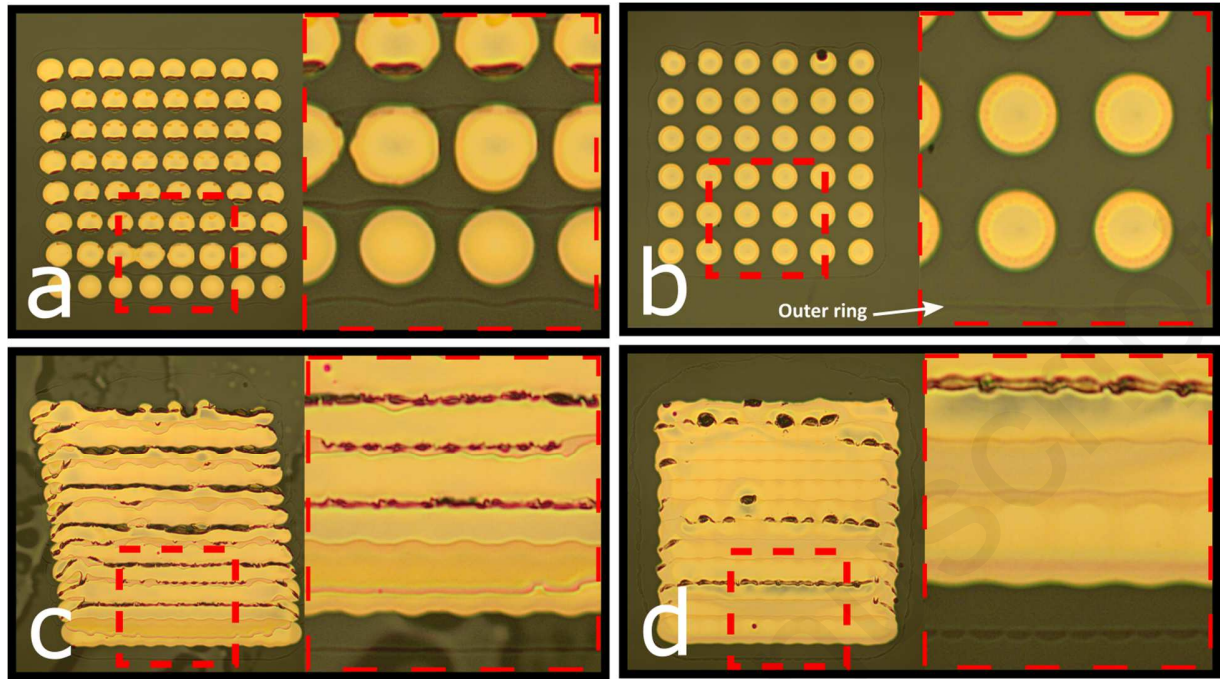


**Figure 7:** Optical pictures of square shaped patterns (approximately  $1 \times 1 \text{ mm}$ ) printed at fixed UV ozone exposure time equals 10 minutes and varying:

i) Jetting frequency equals: 20Hz and 3340Hz, shown in column 1 and 2, respectively; Note that, these values corresponds to the lowest and highest available printing velocities.

ii) drop spacing in order to print: isolated droplets matrix and, continues patterns shown in row 1 and 2, respectively. Drop spacing experimental values equals: a)  $180 \mu\text{m}$ ; b)  $180 \mu\text{m}$ ; c)  $100 \mu\text{m}$ ; d)  $100 \mu\text{m}$ .

## SUPPORTING MATERIALS

### 1. Figures

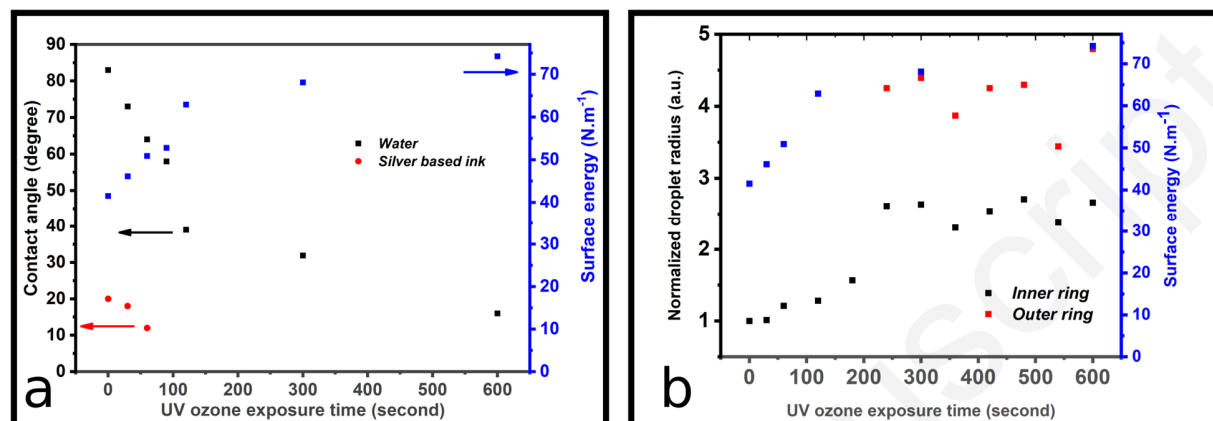


**Figure S1:** Spreading and wetting behavior of the droplets a) Water contact angle and silver based ink contact angle (left axis) as function of UV ozone exposure time . Note that, after 60 seconds silver based ink wets the surface totally and contact angle could not be measured. Surface free energy as function of UV ozone exposure time is plotted on right axis. Values confirm that the more the Su8 surface is exposed to UV ozone treatment, the more the surface becomes hydrophilic. b) Normalized droplet radii (inner and outer rings) and surface energy as function of UV ozone exposure time. The normalized radius show that the inner ring is about 2.5 times larger after 600s of exposure to UV ozone. The outer ring radius remains relatively consistent from its appearance (after 240s) to 600s exposure time.

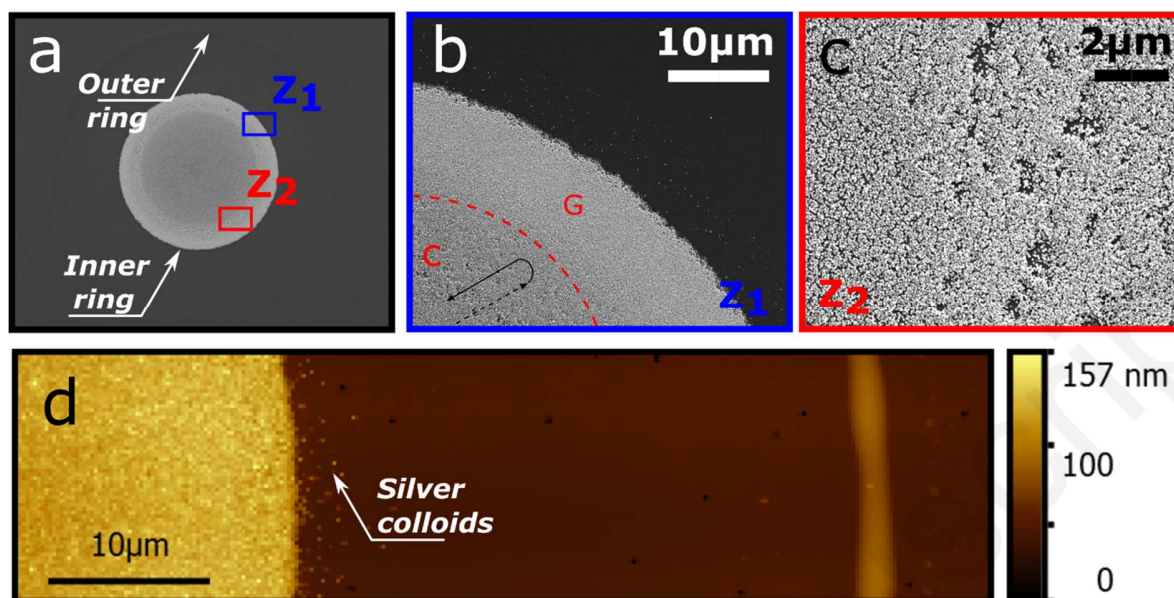


**Figure S2:** SEM pictures showing: a) dried droplet, b) A zoom Z1 showing the border between cap and foot; cap is divided in two regions named C and G. foot is the darkest region of the image; Black arrows shows internal flow in the C region during drying. c) A zoom Z2 showing inhomogeneity of dried nanoparticles in C region. d) AFM scan showing: colloid rich region (yellow region on left side of image) and polymer rich region (right side of the image). AFM image shows the only few amount of silver colloids can be found at the border of colloid and polymer rich region.

**Discussion:** Zoom in SEM optical observations performed at the border between the cap and the foot (Z1) and inside the cap (Z2) provide deeper information about microscopic structure of colloids after drying. In Z1, two regions can be clearly distinguished. “G mark” shows a region where colloids are densely packed. This region forms a band at the periphery of the cap. Inside the cap (region marked C), colloids show less densely packed structure. We suggest that during drying a gel band is formed where there is no flow. In the C region, radial circulation flow occurs however colloids can’t go through the gel band towards the foot. Consequently, coffee stain occurs inside the C regions (see in figures 2c and 2f). Such hypothesis is in good agreement with literature.<sup>[40]</sup>

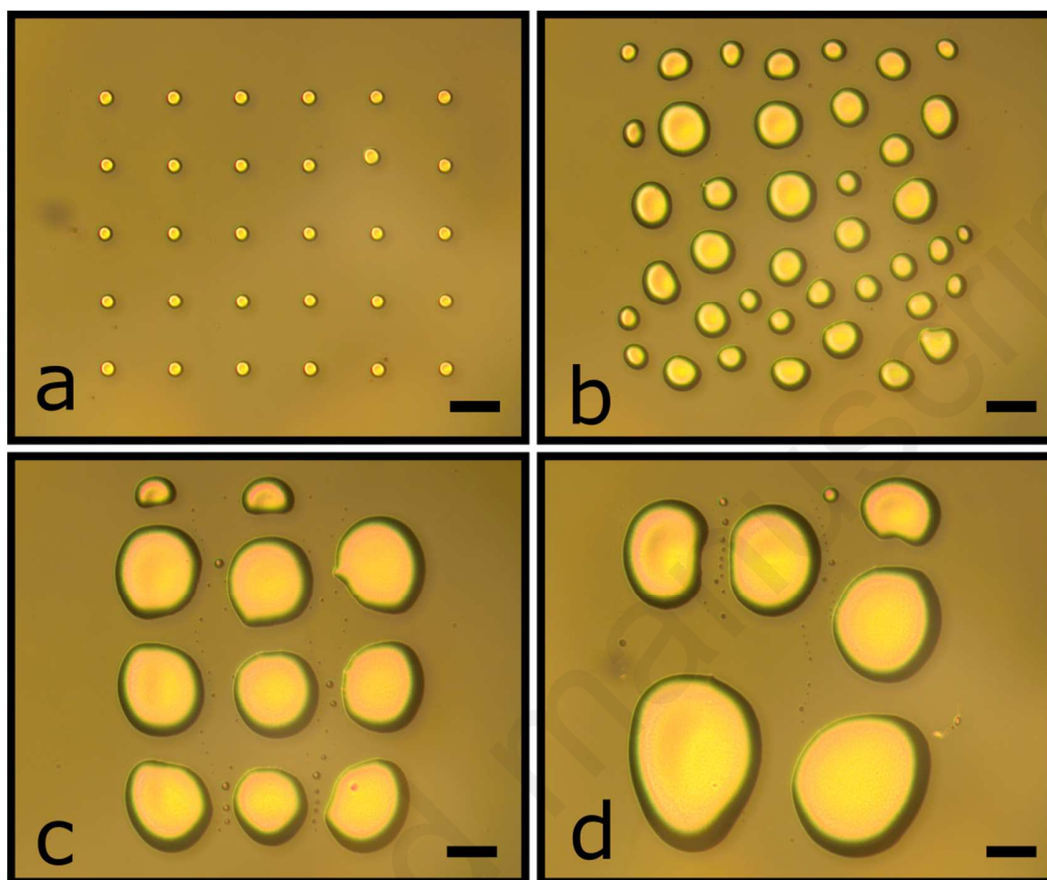


**Figure S3:** Square shaped patterns printed on polymeric surface (Su8 2000.5 MicroChem) without UV ozone treatment. Jetting frequency equals 1KHz and drop spacing equals: a) 100  $\mu\text{m}$  leading to isolated droplets, b) 20  $\mu\text{m}$ , c) 10 $\mu\text{m}$ , d) 5 $\mu\text{m}$ . In images b), c) and d), the printing parameters have been adjusted to overlap adjacent droplet leading to the coalescence of droplets and the formation of a stable pattern.

Scale bars equal 50 $\mu\text{m}$ .

Matrix of isolated droplet is obtained in figure a) because drop spacing (I.e., the distance between the centers of two adjacent droplets) is higher than droplet diameter. Figures S3b, 3c and 3d shows

non-continuous patterns even if drop spacing is lower than droplets diameter. Such phenomena is due to fluid instability on hydrophobic surfaces when triple contact line is not firmly pinned.

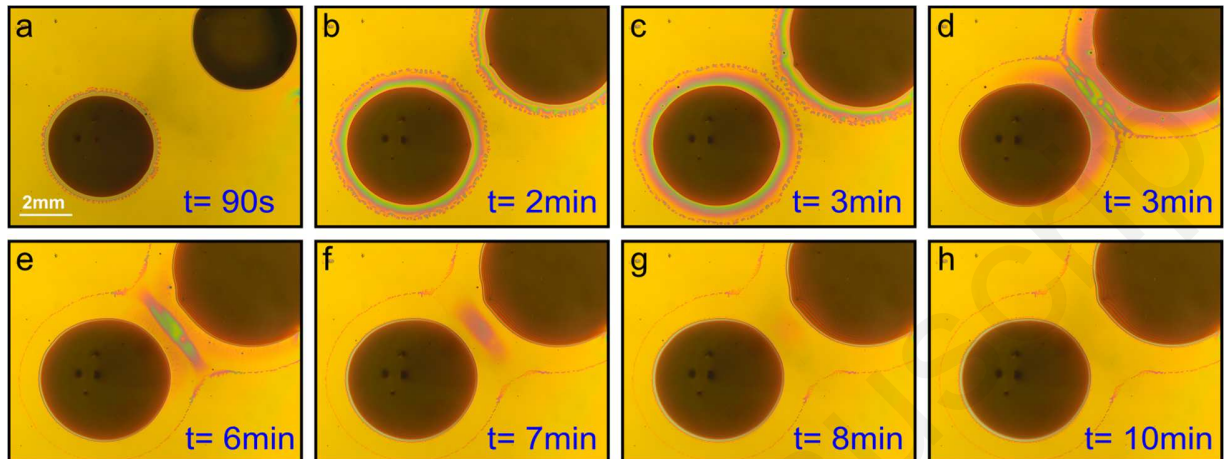


**Figure S4:** Optical images of two droplets successively drop casted on Su8 surface exposed to 6 minutes UV ozone as function of time. Droplet in the bottom left has been deposited at first. Images a to c show that the two droplets spread with same mechanism than for isolated droplet. In image d, the two contact line collapse and form the same outer ring than this one observed when droplet are printed. Images e to h show the drying step of polymer rich region.

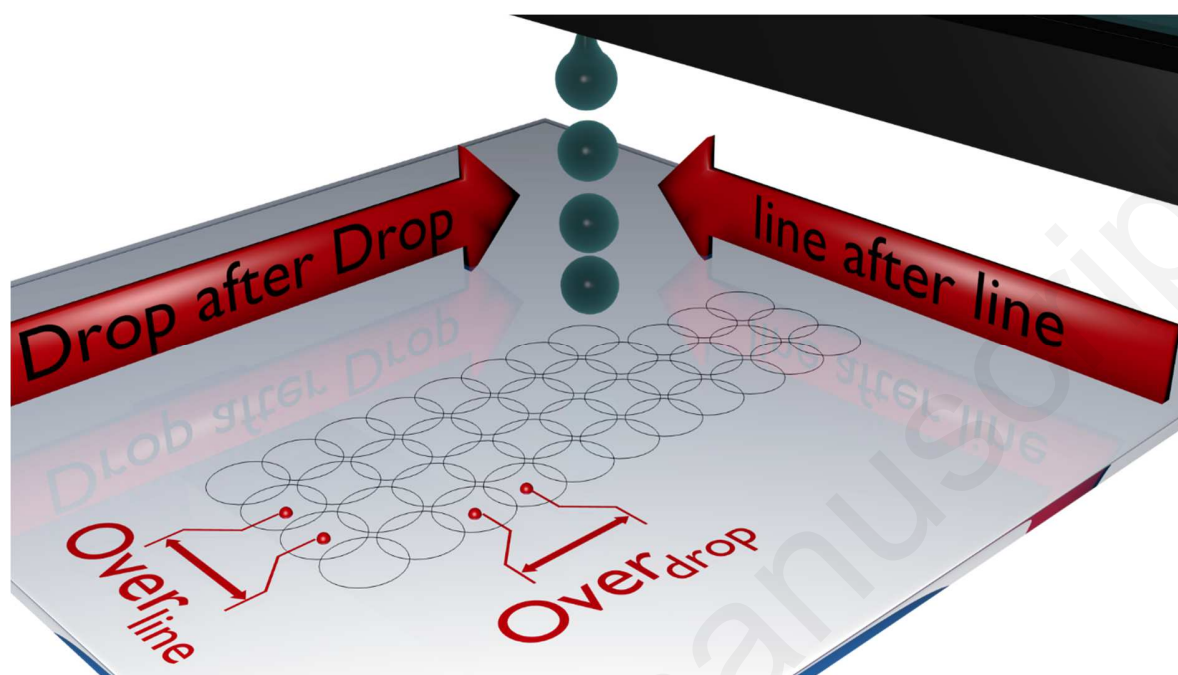


**Figure S5:** 3D scheme showing working principle of DoD inkjet printing for square shaped patterns.  $Over_{drop}$  is relative to droplets spacing that coalesce to form a line.  $Over_{line}$  is relative to line spacing parameters in order to form square shaped patterns. Note that “Drop after Drop” and “line after line” are relative to X axis displacement and Y axis displacement, respectively. Note that the black circle does not highlight materials such as silver colloids, but the three-phase contact line of a dried droplet.

## 2. Videos

**Video S1:** 20s-movie at 25 frame/s showing jetting of silver based in droplets that respect jettable criterions.

## **ACKNOWLEDGMENTS**

This work is supported by the European Union through the European Regional Development Fund (ERDF), and by the French region of Brittany (project: IMPRIM').

Conflict of interest:

The authors declare that they have no conflict of interest.

## **AUTHOR INFORMATION**

### **Corresponding Author**

\* E-mail: maxime.harnois@univ-rennes1.fr

### **Notes**

The authors declare no competing financial interest.

### **Author Contributions**

All authors have given approval to the final version of the manuscript.

## References:

- 1 D. Li, W. Y. Lai., Y.Z. Zhang, W. Huang, (2018). *Adv. Mater.* 30 (2018), 1704738.
- 2 L. Zhou, M. Yu, X. Chen, S. Nie, W.-Y. Lai, W. Su, Z. Cui, W. Huang, *Adv. Funct. Mater.* (2018), 28, 1705955.
- 3 L. Zhou, L. Yang, M. Yu, Y. Jiang, C.-F. Liu, W.-Y. Lai, W. Huang, *ACS Appl. Mater. Interfaces*, 9, (2017), 46, 40533–40540.
- 4 T. Cheng, Y. Wu, X. Shen, W. Lai, W. Huang, *J. Semicond.* (2018), 39, 015001.
- 5 B. Derby, *J. Eur. Ceram. Soc.* 31 (2011) 2543-2550.
- 6 M. Singh, H. M. Haverinen, P. Dhagat, G. E. Jabbour *Adv. Mater.* 22 (2010) 673-685.
- 7 M. Medina-Sánchez, C. MartínezDomingo, E. Ramon, A. Merkoçi, *Adv. Funct. Mater.* 24 (2014) 6291-6302.
- 8 D. Kwak, J. A. Lim, B. Kang, W. H. Lee, K. Cho, *Adv. Funct. Mater.* 23 (2013) 5224-5231.
- 9 R. Malo, W. Kuai, M. Amela-Cortes, S. Cordier, Y. Molard, T. Mohammed-Brahim, E. Jacques, M. Harnois, *ACS Appl. Mater. Interfaces* 7 (2015) 21975-21984;
- 10 C. Avis, H.R. Hwang, J. Jang, *ACS Appl. Mater. Interfaces* 6 (2014) 10941-10945.
- 11 H. L., Gomes, M.C.R. Medeiros, F. Villani, J. Canudo, F. Loffredo, R. Miscioscia, C. Martinez-Domingo, E. Ramon, E. Sowade, K.Y. Mitra, R.R. Baumann, I. McCulloch, J. Carrabina, *Microelectron. Reliab.* 55 (2015) 1192-1195
- 12 F.C. Krebs, *Sol. Energy Mater. Sol. Cells* 93 (2009) 394-412.
- 13 R. Rogel, B. Le Borgne, T. Mohammed-Brahim, E. Jacques, M. Harnois, *Adv. Mater. Interfaces* 4 (2017) 1600946.
- 14 Le Borgne, B., De Sagazan, O., Crand, S., Jacques, E., Harnois, M. (2017). *ACS Appl. Mater. Interfaces*, 9(35), 29424-29429.
- 15 S.H. Huang, P. Liu, A. Mokasdar, L. Hou, *Int J Adv Manuf Technol.* 67 (2013) 1191–1203.
- 16 M. Vaezi, H. Seitz, S. Yang, *Int J Adv Manuf.* 67 (2013) 1721–1754.
- 17 P. Calvert, *Chem. Mater.* 13 (2001) 3299-3305.
- 18 B.J. Gans, P.C. Duineveld, U.S. Schubert, *Adv. Mater.* 16 (2004) 203–213.
- 19 E. Tekin, P.J. Smith, U.S. Schubert, *Soft Matter.* 4 (2008) 703-713.
- 20 H.C. Nallan, J.A. Sadie, R. Kitsomboonloha, S.K. Volkman, V. Subramanian, *Langmuir* 30 (2014) 13470-13477.
- 21 H.H. Lee, K.S. Chou, K.C. Huang, *Nanotechnology* 16 (2005) 2436-2441.
- 22 M. Grouchko, A. Kamyshny, S. Magdassi, S. J. Mater. Chem. 19 (2009) 3057-3062.
- 23 C. Sire, F. Ardiaca, S. Lepilliet, J.W.T Seo, M.C. Hersam, G. Dambriane, H. Happy V. Derycke, V. Nano Lett. 12 (2012) 1184-1188.
- 24 H. Sirringhaus, T. Kawase, R.H. Friend, T. Shimoda, M. Inbasekaran, W. Wu, E.P. Woo, *Science* 290 (2000) 2123-2126.
- 25 T. Shimoda, K. Morii, S. Seki, H. Kiguchi, *MRS Bull.* 28 (2003) 821-827.
- 26 S.H. Eom, S. Senthilarasu, P. Uthirakumar, S.C. Yoon, J. Lim, C. Lee, S.H Lee, *Org. Electron.* 10 (2009) 536-542.
- 27 H. Minemawari, T. Yamada, H. Matsui, J.Y. Tsutsumi, S. Haas, R. Chiba, T. Hasegawa, *Nature* 475 (2011) 364-367.
- 28 K.E. Paul, W.S. Wong, S.E. Ready, R.A. Street, *Appl. Phys. Lett.* 83 (2003) 2070-2072.
- 29 J. Li, F. Ye, S. Vaziri, M. Muhammed, M.C. Lemme, M, *Adv. Mater.* 25 (2013) 3985-3992.
- 30 P. Calvert, *Chem. Mater.* 13 (2001) 3299– 3305.
- 31 B.J. De Gans, E. Kazancioglu, W. Meyer, U.S. Schubert, *Macromol. Rapid Commun.* 25 (2004) 292– 296
- 32 D. Jang, D. Kim, J. Moon, *Langmuir* 25 (2009) 2629– 2635,
- 33 J. Stringer, B. Derby, *Langmuir* 26 (2010) 10365-10372.
- 34 D. Soltman, V. Subramanian, *Langmuir* 24 (2008) 2224-2231.
- 35 R.D. Deegan, O. Bakajin, T.F. Dupont, G. Huber, S.R. Nagel, T.A. Witten, *Nature* 389 (1997) 827– 829

- 36 H. Hu, R.G. Larson, *J. Phys. Chem. B* 110 (2006) 7090–7094.
- 37 P. Duineveld, C. Paul, *J. Fluid. Mech.* 477 (2003) 175-200.
- 38 J. Park, J. Moon, *Langmuir* 22 (2006) 3506-3513.
- 39 A. Kamyshny, J. Steinke, S. Magdassi, *Open App. Phys. J.* 4 (2011) 19-36.
- 40 M.D. Haw, M. Gillie, W.C.K. Poon, *Langmuir* 18 (2002) 1626-1633.
- 41 Y.Y. Tarasevich, D.M. Pravoslavnova, *Eur. Phys. J.* 22 (2007) 311-314.
- 42 F. Parisse, C. Allain, *Journal de Physique II, EDP Sciences* 6 (1996) 1111-1119.
- 43 S. Keller, G. Blagoi, M. Lillemose, D. Haefliger, A. Boisen, *J. Micromech. Microeng.* 18 (2008) 125020-125030.
- 44 S. J. Moon, M. Robin, K. Wenlin, M. Yann, B. S. Bae, T. Mohammed-Brahim, E. Jacques, M. Harnois, *Flex. Print. Electron.* 2 (2017) 035008-035017.
- 45 J. Doggart, Y. Wu, P. Liu, S. Zhu, *ACS Appl. Mater. Inter.* 2 (2010) 2189-2192.
- 46 M. Allen, J. Leppäniemi, M. Vilkmann, A. Alastalo, T. Mattila, *Nanotechnology* 21 (2010) 475204-475210.
- 47 H. Andersson, A. Manuilskiy, C. Lidenmark, J. Gao, T. Öhlund, S. Forsberg, J. Oertegren, W. Schmidt, H. E. Nilsson, *Nanotechnology* 24 (2013) 455203-455213.
- 48 P. Müller-Buschbaum, D. Magerl, R. Hengstler, J.-F. Moulin, V. Körstgens, A. Diethert, J. Perlich, S. V. Roth, M. Burghammer, C. Riekkel, M. Gross, F. Varnik, P. Uhlmann, M. Stamm, J. M Feldkamp, C. G. Schroer. *J. of Phys.: Condens. Matter*, 23 (2011), 184111.
- 49 S. V. Roth, A. Rothkirch, T. Autenrieth, R. Gehrke, T. Wroblewski, M. C. Burghammer, C. Riekkel, L. Schulz, R. Hengstler, P. Müller-Buschbaum. *Langmuir*, 26, (2009), 1496-1500.
- 50 S. V. Roth, A. Rothkirch, T. Autenrieth, G. Grübel, C. Riekkel, M. Burghammer, R. Hengstler, R. Hengstler, L. Schulz, P. Müller-Buschbaum, *Appl. Phys. Lett.* 91, (2007), 091915.